27

BULLETIN Of the International Association of ENGINEERING GEOLOGY de l'Association Internationale de GÉOLOGIE DE L'INGÉNIEUR No 47 PARIS 1993

APPLYING THE LAGAMINE MODEL TO COMPUTE LAND SUBSIDENCE IN SHANGHAI

APPLICATION DU MODÈLE LAGAMINE AUX PROBLÈMES DE TASSEMENT À SHANGHAÏ

A. DASSARGUES*, Ch. SCHROEDER* and X.L. LI**

Introduction

The first studies of the subsidence phenomena using models based on physical concepts, were semi-infinite elastic solid models which assume the soil to behave like a homogeneous, isotropic half space with a uniform elasticity modulus. More rigorous approaches have followed and have contributed to significant improvements in "subsidence modelling" especially thanks to models including transient flow with coupled or partially coupled laws.

The model used herein (Charlier *et al.*) could be qualified of a "two-step" method according to Corapcioglu (1984). The aquifer flow equation is solved in a three-dimensional space and the assumed one-dimensional solid deformation is computed by one-dimensional consolidation equations.

The results of the 3D flow model are the time dependent boundary conditions for the 1D consolidation model. This consolidation model uses the oedometric elasto-plastic law coupled with vertical flow, including linear or non-linear analysis of the vertical permeability.

This paper will present the computational schema, the preparation of the data and the way they have been entered in the 3D flow model and in the flow-compaction model.

Computational schema (Fig. 1)

The permeability contrast between aquifers and aquitards (Dassargues *et al.*, 1989) is such that the main groundwater flows due to pumping can be considered as essentially influenced by horizontal transmissivities of the confined aquifers.

This fact has led to the choice of the following computational schema :

- The flow model is a real 3D model (Dassargues *et al.* 1988) with a complete discretization of the different layers in the mesh, many values of the parameters (K and S_s) being chosen in the different elements to ensure a very detailed spatial distribution. The result of this transient model consists in the spatial distribution of the computed water pressures as a function of time. But the values relative to clayey layers are not very accurate because of the very low permeability coefficients.
- The subsidence computations are completed, coupling in the model the vertical flow and the oedometric (elastoplastic) consolidation process in the clayey layers.
- As mentioned above, the pore-pressures computed in the 3D model are introduced into the coupled model as prescribed variable pressures at the aquifer-aquitard boundaries.

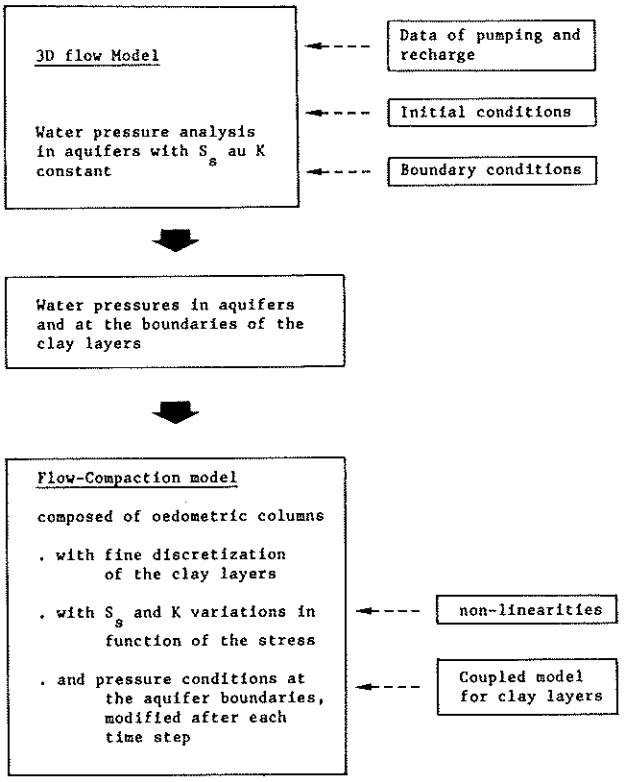

Fig. 1 : Computational schema.

* Laboratoires de Géologie de l'Ingénieur, d'Hydrogéologie et de Prospection Géophysique, Université de Liège, Liège, Belgique.
** Shanghai Station of Environmental Geology, Shanghai, P.R. China. Now at the M.S.M. department, University of Liège, Liège, Belgique.

Preparation of the data

A. Geomechanical data

It appears that complex and variable sedimentological conditions have led to a geometrically complex distribution of the different geological units. This fact will strongly influence the value of the compaction in the different zones. For the clayey layers, values of the effective preconsolidation stress, compression index (C_c), void ratio (e) and vertical permeability coefficient (k_z) are obtained from oedometer and identification tests performed between 1960 and 1985 at the Shanghai Geological Center.

Results (Schroeder *et al.*, 1990) have shown that the *first, second and third compressible layers* are very slightly overconsolidated and the DGSC layer strongly overconsolidated. The overconsolidation of the compressible layers is probably due to the consolidation which has occurred between 1920 and 1965 (during the main subsidence).

Initial conditions of 1920 are chosen in perfect equilibrium with a triangular distribution of the initial effective stress (σ'_i), obtained when assuming total saturation of the layers (Fig. 2). In the computations, the preconsolidation effective stress (σ'_{prec}) is assumed to be equal everywhere to the initial effective stress except in the DGSC layer which is considered overconsolidated in 1920 with a mean ratio

$$\frac{\sigma'_{prec}}{\sigma'_i} = 1.4$$

For aquifer and compressible layers, we assume :

$$\sigma'_{prec} = \sigma'_i = (\gamma - \gamma_w) \cdot H \qquad (1)$$

where H = depth
σ'_i = initial effective stress
γ = bulk density.

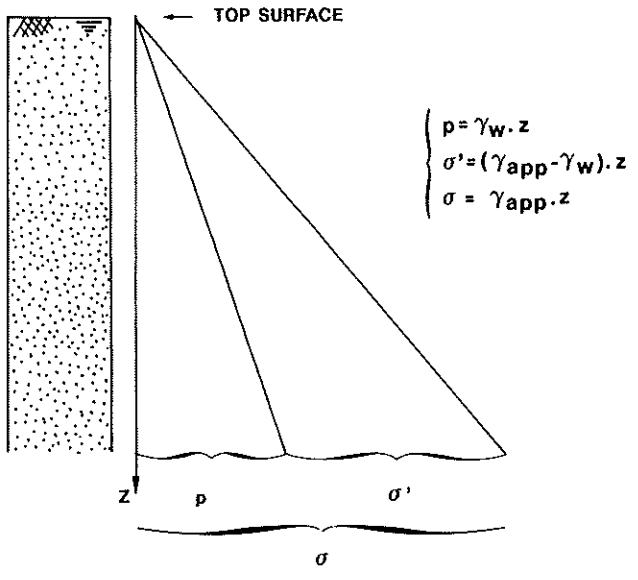

Fig. 2 : Initial conditions of stress.

Table 1 : Variation range for the C_c values.

Layer	Range of C_c	
Phreatic aquifer	0.04	0.09
First compresible layer	0.4	1.2
Second compressible layer	0.3	1.2
D.G.S.C.	0.2	0.4
First aquifer	0.2	0.3
Third compressible layer	0.3	0.5
Second aquifer	0.15	0.2

On the basis of all the results of the oedometer tests, C_c and C_s have been determined. Other values of the identification properties, like w_L (liquid limit), I_p (plasticity index), γ_d (density) and w (water content), have helped to check the reliability of the data provided by the oedometer tests. Indeed, many empirical relations linking all these properties have been observed by many authors (Terzaghi, Skempton,...).

The results of all the tests have been confronted to these empirical relations and observed trends. On the basis of these relations and trends, we have determined the range of variation of the C_c values for the different formations of the subsoil of Shanghai (Table 1).

For computation of the subsidence, the values of A (swelling constant) and C (compression constant) are also determined from C_s, C_c and initial void ratio of 1920 (e_i) using :

$$A = 2.3 \frac{(1 + e_i)}{C_s} \qquad (2)$$

$$C = 2.3 \frac{(1 + e_i)}{C_c} \qquad (3)$$

This initial void ratio is deduced from the relation :

$$e_i = \Delta e + e_o \qquad (4)$$

where e = void ratio determined by the geotechnical tests on the samples
Δe = variation of the void ratio between 1920 and the date of sampling

In the case of normally consolidated layers (*first, second and third compressible layers, first and second aquifers*) Δe is determined by :

$$\Delta e = C_c \log \frac{(\sigma'_i + \Delta\sigma')}{\sigma'_i} \text{ (plastic part)} \qquad (5)$$

In the case of the *DGSC layer* :

$$\Delta e = C_c \log \left(\frac{\sigma'_i + \Delta\sigma'}{\sigma'_i} \right) \text{ (elastic part)} \qquad (6)$$

if $\Delta\sigma' < (\sigma'_{prec} - \sigma'_i)$

or

$$\Delta e = C_s \log \left(\frac{\sigma'_{prec}}{\sigma'_i} \right) + C_c \log \left(\frac{\sigma'_i + \Delta\sigma'}{\sigma'_{prec}} \right) \qquad (7)$$

(elastic and plastic parts)

if $\Delta\sigma' > (\sigma'_{prec} - \sigma'_i)$

A difference of about 20 % in the void ratio is determined between 1920 and 1965 in the compressible layers.

B. Variation of the hydrodynamic parameters during compaction

In soil consolidation problems, the compaction flow is described more realistically if the specific storage (S_s) and permeability coefficient (K) can vary with effective stress (σ'). These variations introduce non-linearities in the coupled flow-compaction equation.

The vertical flow-consolidation equation can be reduced to (De Marsily, 1981) :

$$\frac{k_z}{\rho \cdot g \cdot m_v} \cdot \frac{\partial^2 p}{\partial z^2} = \frac{\partial p}{\partial t} + q' \qquad (8)$$

where p = water pressure
z = vertical coordinate
q′ = external sink or source term
$p \cdot g = \gamma_w$ = unit weight of the water
$m_v = (n\beta - n\beta_s + \alpha)$
with β = compressibility coefficient of the liquid
β_s = compressibility coefficient of the solid
α = compressibility of the porous media due to the decrease of porosity

For the variation of permeability, many relations are used, corresponding in each case to particular lithological and geotechnical conditions. For Shanghai sediments, tests have shown the Nishida and Nakagawa (1969) equation to be the best empirical relation. Based on extensive experimental results on various estuarine, recent marine clays, the relation linking the permeability K to void ratio e and plasticity index I_p is :

$$e = a + b \cdot \log_{10} k \qquad (9)$$

where $a = 10 \cdot b$
$b = 0.01\ I_p + 0.05$
k = permeability in cm/sec

If K is expressed in m/sec, entering the value of a in the equation, we obtain :

$$K = \exp(\alpha_N \cdot e + \beta_N) \qquad (10)$$

where $\alpha_N = \frac{2.3}{b}$ and $\beta_N = (-27.6)$

The value of α_N, depending on I_p, can characterize each clayey layer. To obtain a more realistic relation in each case, the b value is generalized :

$$b = C + D \cdot I_p$$

where C and D are constants adopted for each layer.

In the studied area of Shanghai, many tests have given a lot of permeability values (by oedometer tests), void ratio and plasticity index. Diagrams of I_p (%) versus b are drawn for clayey layers and a linear regression allows the determination of C and D; we obtain :

- *first compressible layer* $b = 0.213 + 0.083\ I_p$
- *second compressible layer* $b = 0.0167 + 0.0174\ I_p$
- *DGSC layer* $b = 0.0885 + 0.0127\ I_p$
- *third compressible layer* $b = 0.176 + 0.079\ I_p$

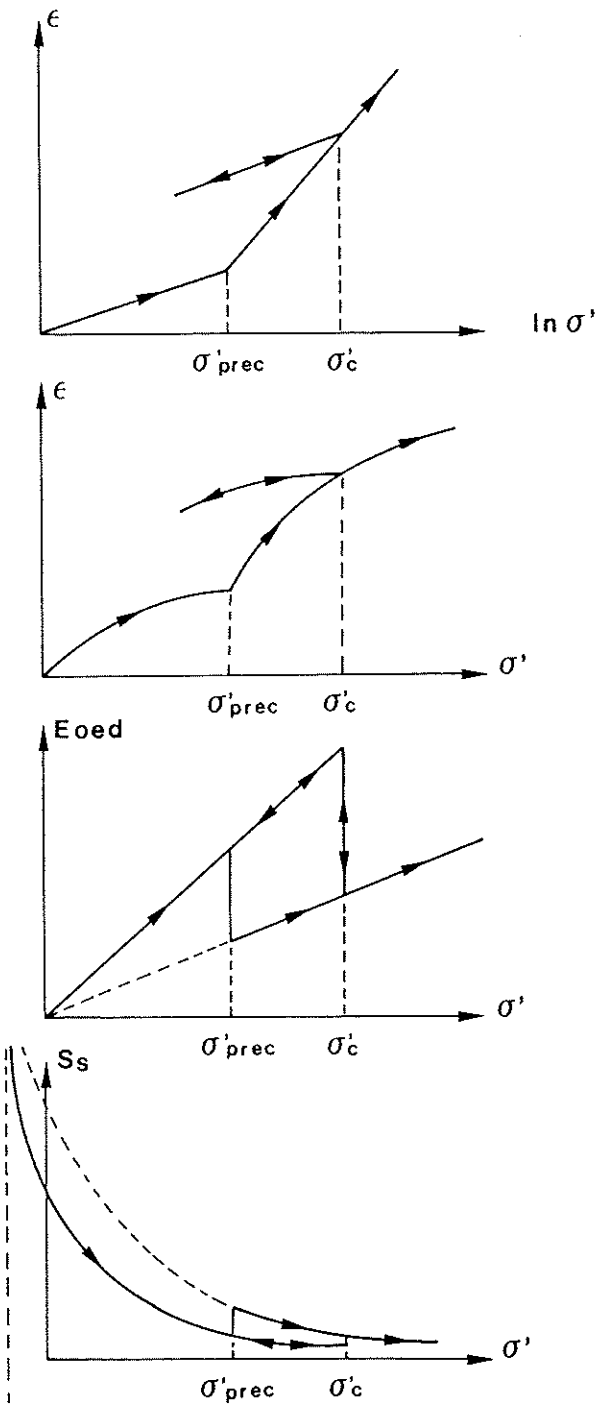

Fig. 3 : Variation of the specific storage S_s.

The value of m_v in the equation (8) is more often determined by oedometer tests assuming Terzaghi's theory (1948)

$$\frac{\partial n}{\partial t} = \frac{1}{1 + e_o} \cdot \frac{\partial e}{\partial t} = m_v \frac{\partial p}{\partial t} \qquad (11)$$

where e_o = void ratio (before testing)

At any moment of the consolidation, m_v varies with p or σ' and, for a loading step, it can be written :

$$m_v = \frac{\Delta e}{(1 + e) \cdot \Delta p} \qquad (12)$$

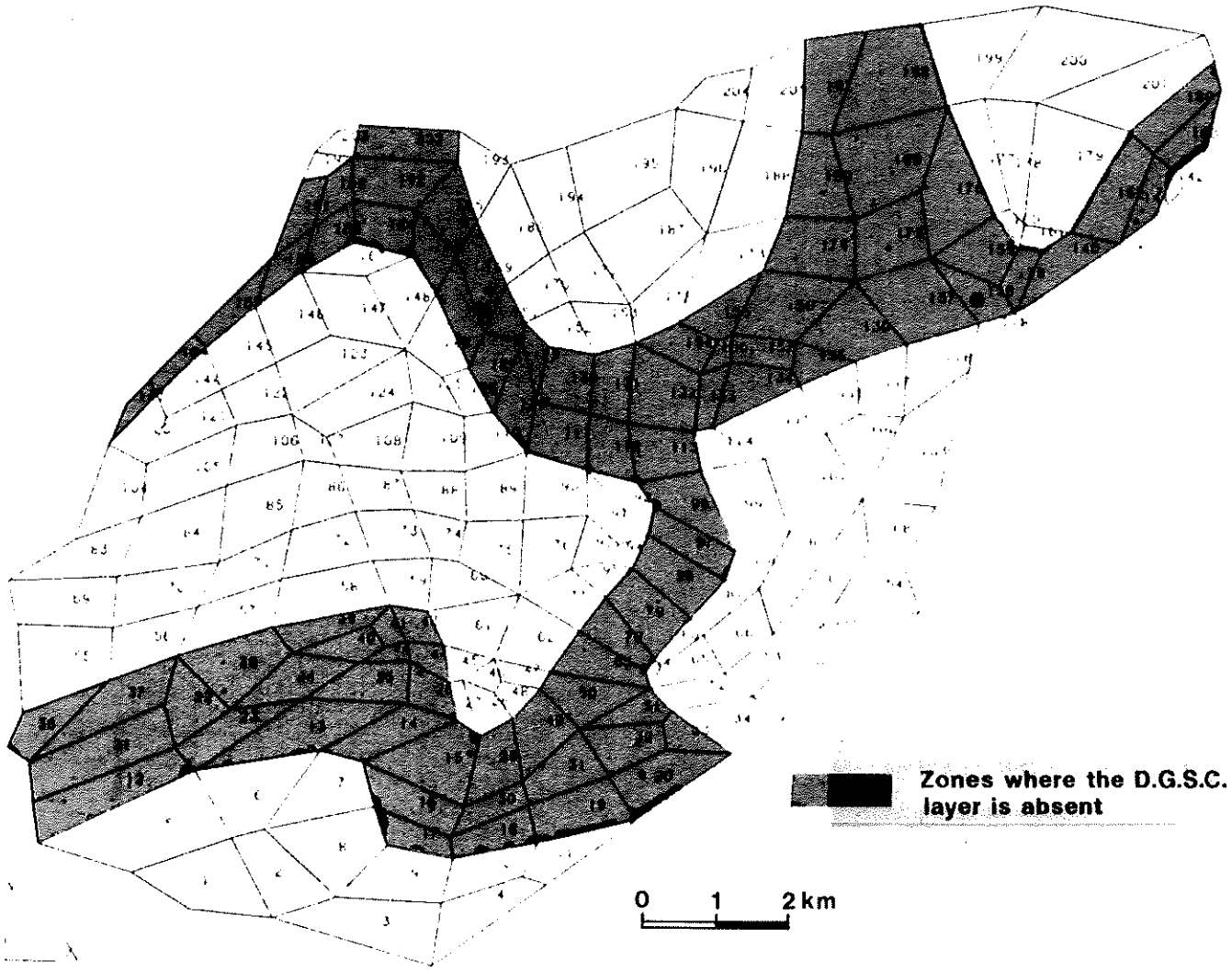

Fig. 4 : Presence or lack of DGSC in the 4th layer of the network.

where e = void ratio at the beginning of the present loading step (Δp).

The general expression of the specific storage is

$$S_s = \rho \cdot g \cdot m_v = \rho \cdot g \cdot n \left(\beta - \beta_s + \frac{\alpha}{n} \right) \quad (13)$$

Usually β and β_s can be neglected with respect to α (Poland, 1984), so that

$$S_s = \rho \cdot g \cdot \alpha \quad (14)$$

$$\text{and} \begin{cases} S_s = \gamma_w / A \cdot \sigma' \text{ (in the elastic part)} \\ S_s = \gamma_w / C \cdot \sigma' \text{ (in the plastic part)} \end{cases} \quad (15)$$

where A is the swelling constant
C is the compression constant

The variation of the specific storage S_s as a function of the effective stress (σ') is clearly apparent on Figure 3. There is a continuous variation of S_s added to a discontinuity corresponding to the effective pre-consolidation stress.

In the coupled flow-compaction law, this variation is taken into account by assuming that the total quantity of water expelled during compaction ($-f^v$) is equal to the time derivation of the deformation ($\dot{\varepsilon}$) (Charlier *et al.*).

Data for the 3D flow model

A. Spatial discretization

3D brick finite elements with 8-nodes are used. Their edges are line segments. The trilinear interpolation functions are written in the intrinsic coordinates; the Jacobian matrix is 3 × 3.

The water pressure variations in the semi-pervious layers will be badly represented if only one or two elements represent the vertical discretization of such layers. In this case, a linear evolution will be found between the lower node and the upper node, not taking

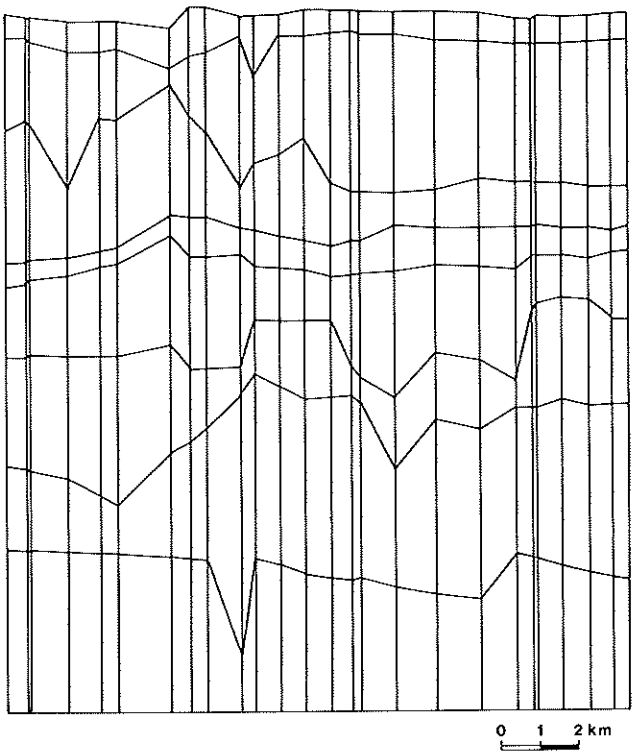

Fig. 5 : Vertical profile.

into account the transient effects due to the low permeability.

For this study (as explained before), the 3D flow model is used essentialy to compute the water pressure in the aquifer as a function of the solicitations of the system. These values will be taken as transient boundary data for the flow-compaction model.

The geometrical 3D mesh must incorporate many geometrical data in the discretization : location of points where data are available, limits of geological units or main changes in the lithological facies.

The different geological formations, distinguished in the upper 70 m of the Shanghai subsoil by Quaternary analysis during the hydrogeological and engineering geology studies, are represented in the model. Separations in the semi-pervious layers are less accurate than for the aquifer layers. The total area is about 129 km^2. To avoid an excessive number of elements, 10 layers of 205 finite elements have been introduced corresponding to a total of 2,070 nodes.

From one level of nodes to the next one, only 2 coordinates are changing. In this way, the numbering of nodes and elements in the discretized structure can be computed from one layer to the next one by simple addition of an increment.

The complexity of the whole discretized structure is very high.

As much as possible, the nodes are placed on existing boreholes where samples were taken or where data are available.

The mesh takes into account all the known geological discontinuities and heterogeneities of the represented volume of loose sediments.

The successive layers are not necessarily horizontal layers. For instance, as shown on Figure 4, the presence or absence of the Dark Green Stiff Clay layer is represented in the 4th layer of the structure.

One of the vertical profiles in the complete meshing network is shown on Figure 5, the location of this profile is on Figure 17.

The spatial distribution of the two parameters (K and S_s) is obtained by introduction of material classes for which the parameters are defined. Each element of the structure is affected by one of the defined classes.

Fourteen classes of materials are used in the model. The spatial distribution of them is shown on Figures 6 to 15 for the whole meshing network.

For these classes, the following lithological correspondance can be summarized as follows :

Material
1 superficial clayey soil
2 upper part : clayey loam
lower part : clay mixed with silty sand
3 clayey loam mixed with silty sand
4 clay with peat
5 clayey loam with peat
6 clay
7 clayey loam
8 sandy loam
9 clayey loam interlayered with silty sand
10 silty sand
11 "Dark Green Stiff Clay" (consolidated clay)
12 fine silty sand
13 clayey loam interbedded with silty sand
14 fine sand

The values of the hydrodynamic parameters corresponding to these classes will be discussed later in the description of the calibration procedure.

B. Time discretization

A solution of the system is found after each time step, this one is a main factor affecting the convergence. The step size must be chosen taking into account :

— the dimension of the modelled area
— the model results as a function of time required for comparison with available measurements. If the measurement data are few, there is no need to have very short time steps
— the expected accuracy of the results as a function of the time.

These three imperatives, confronted with the available data of this study, the pumping characteristics and the expected accuracy, have led to the choice of the following time-discretization :

— from 1870 to 1920.75* : few time steps following a geometrical progression to initialize the problem

* 1920.75 corresponds to the date : October 1st, 1920.

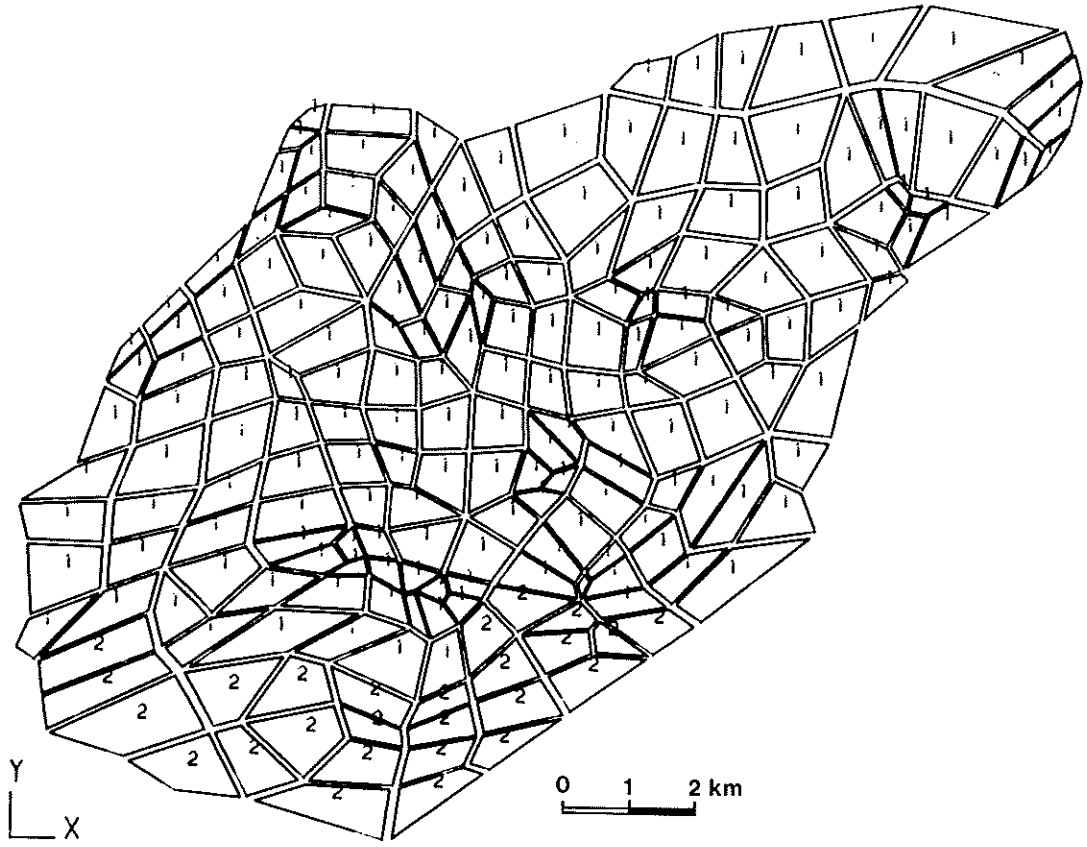

Fig. 6 : 1st layer of elements.

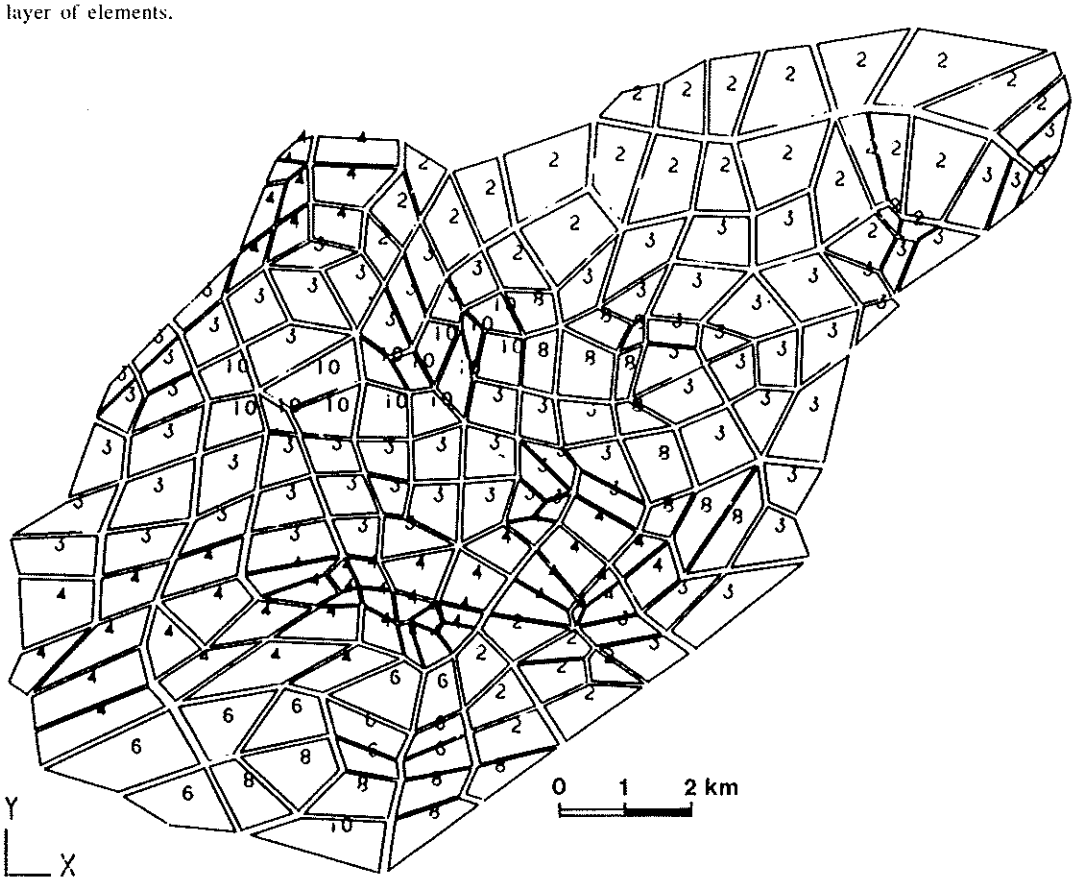

Fig. 7 : 2nd layer of elements.

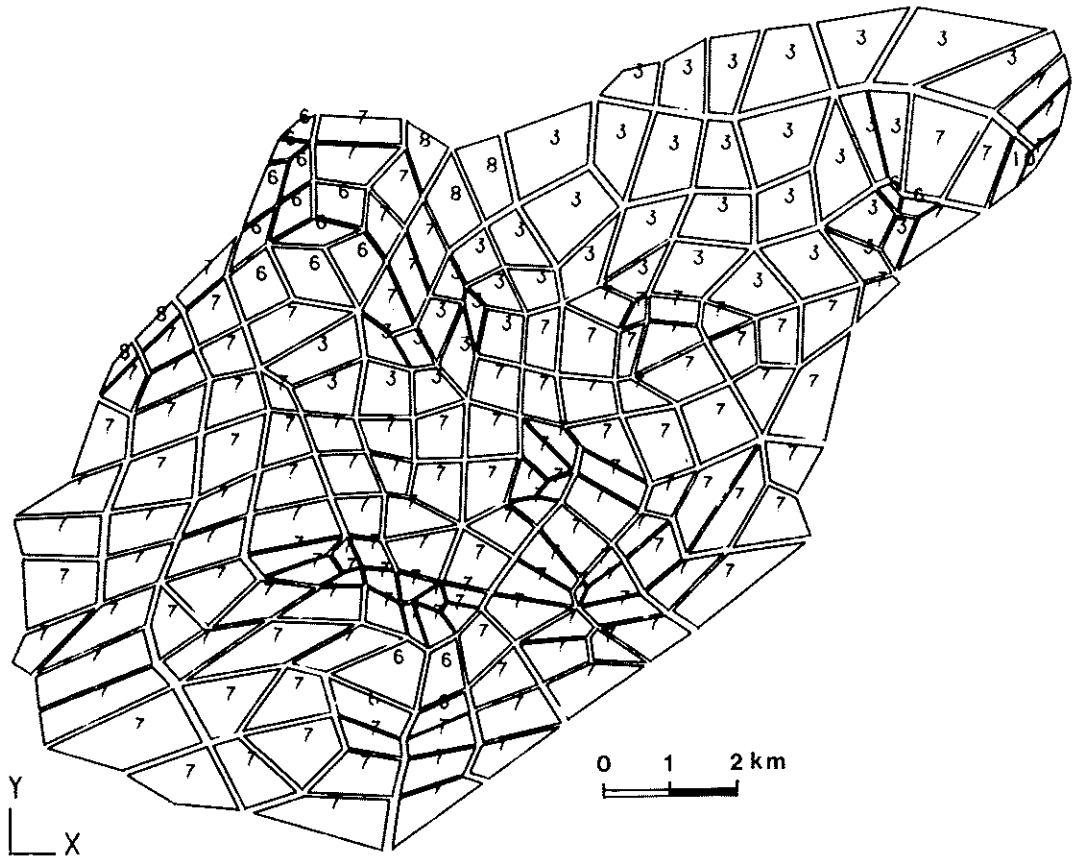

Fig. 8 : 3rd layer of elements.

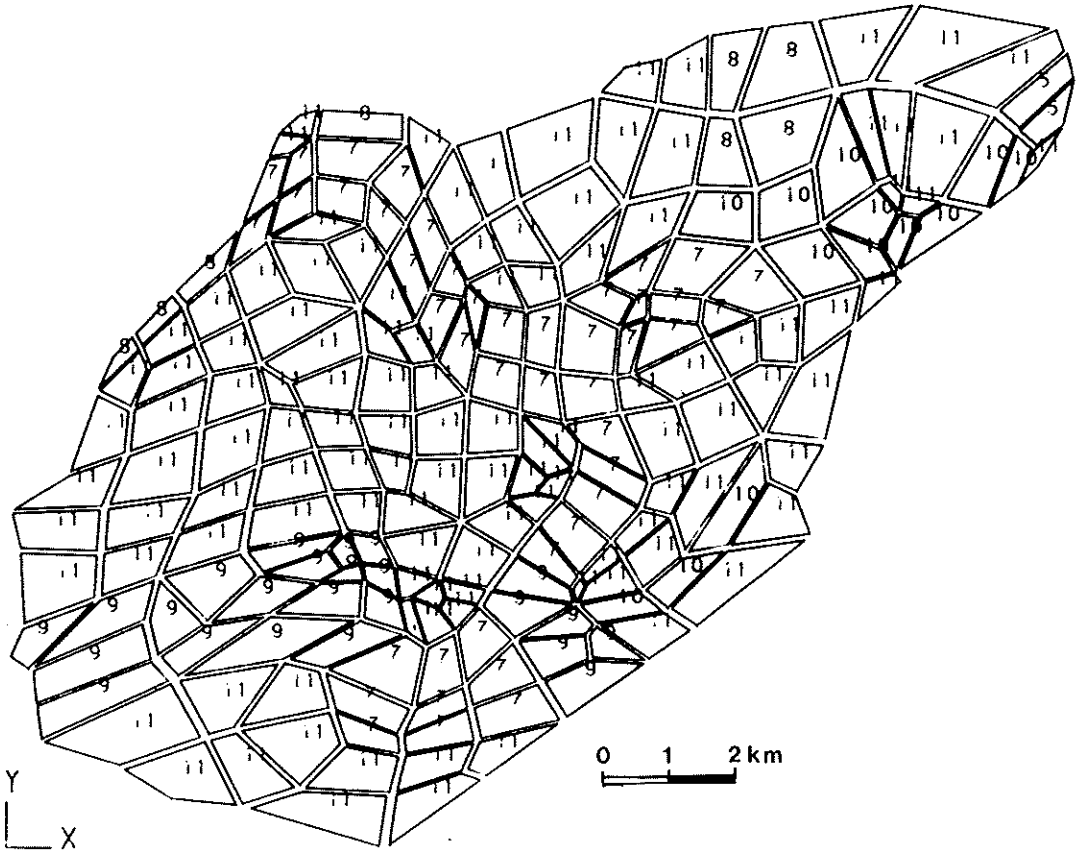

Fig. 9 : 4th layer of elements.

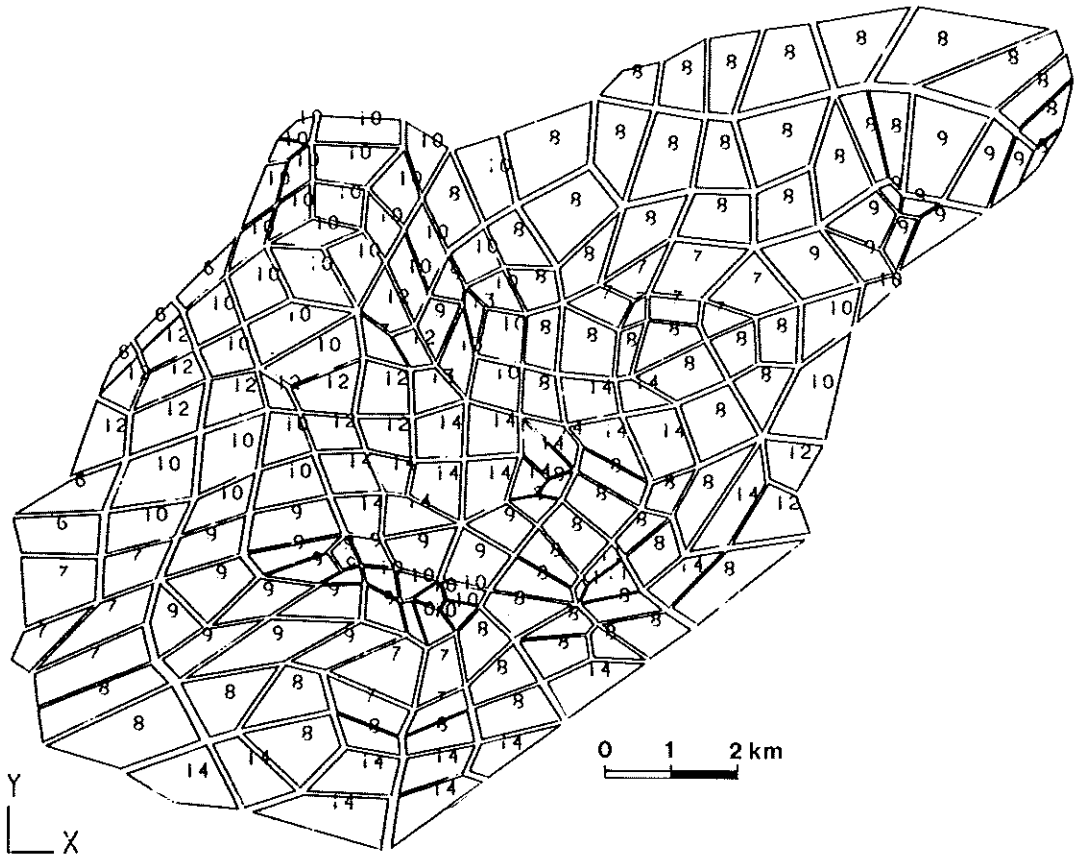

Fig. 10 : 5th layer of elements.

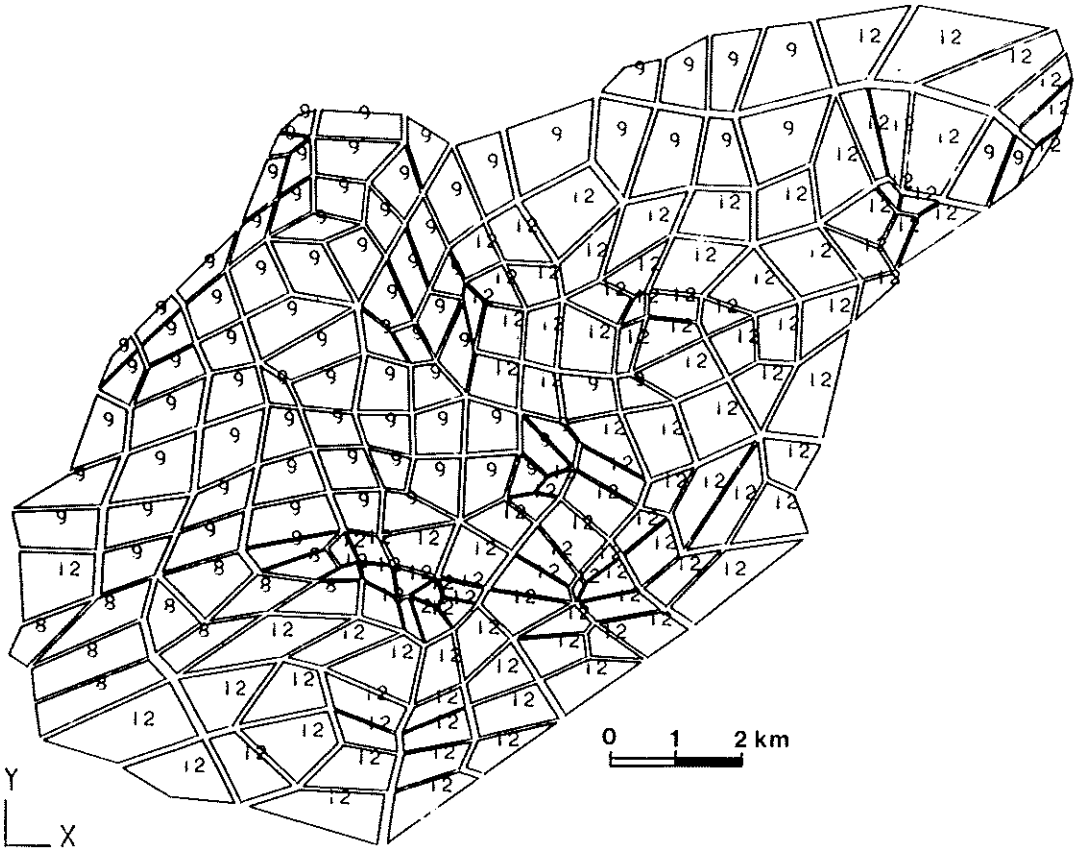

Fig. 11 : 6th layer of elements.

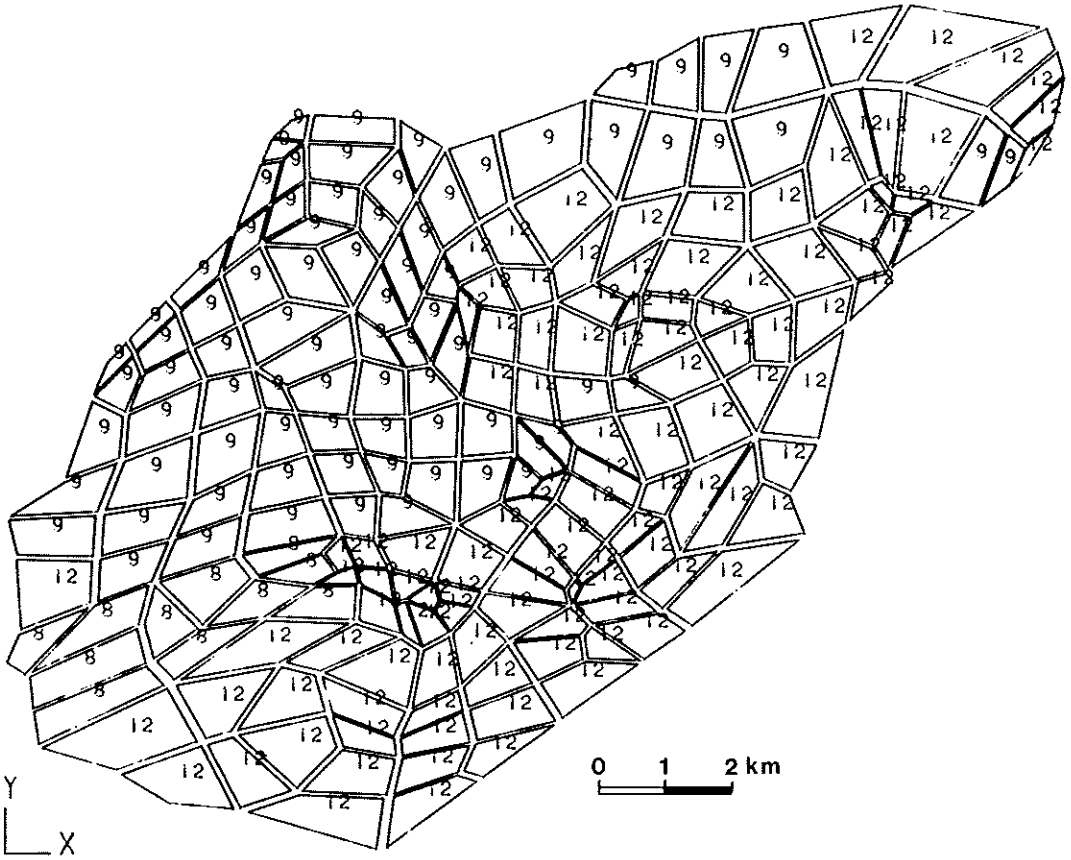

Fig. 12 : 7th layer of elements.

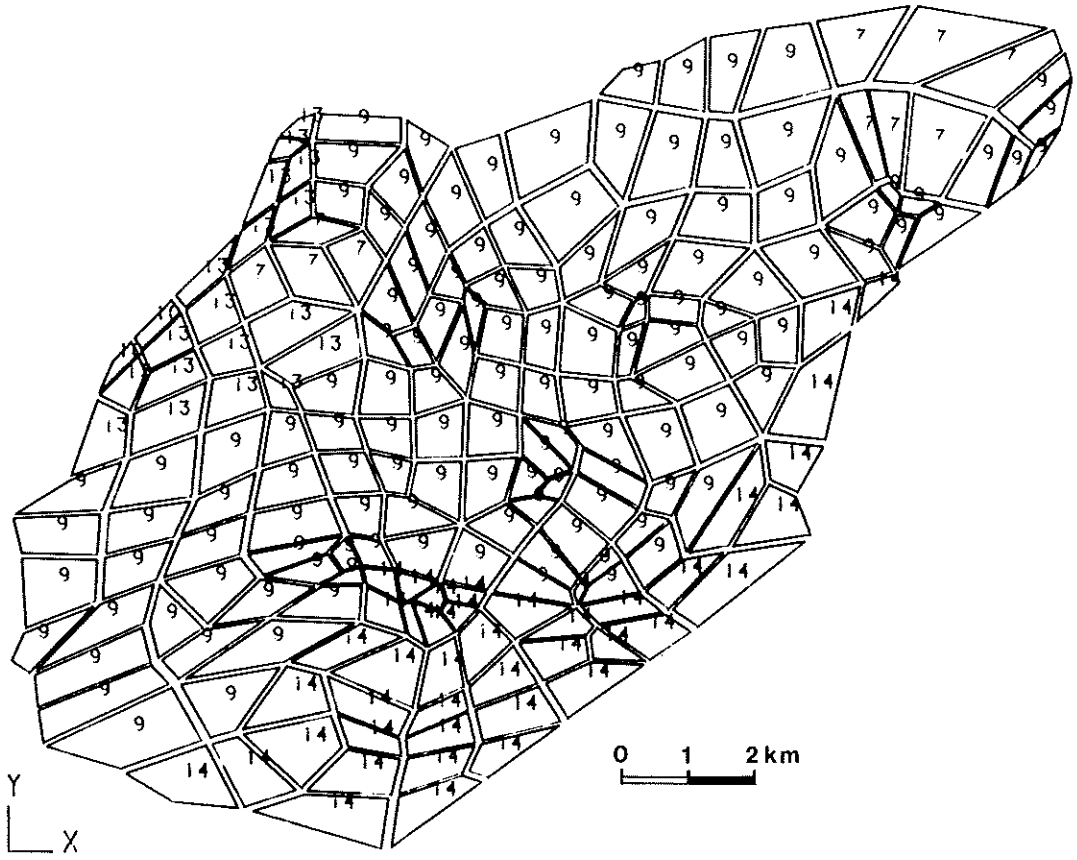

Fig. 13 : 8th layer of elements.

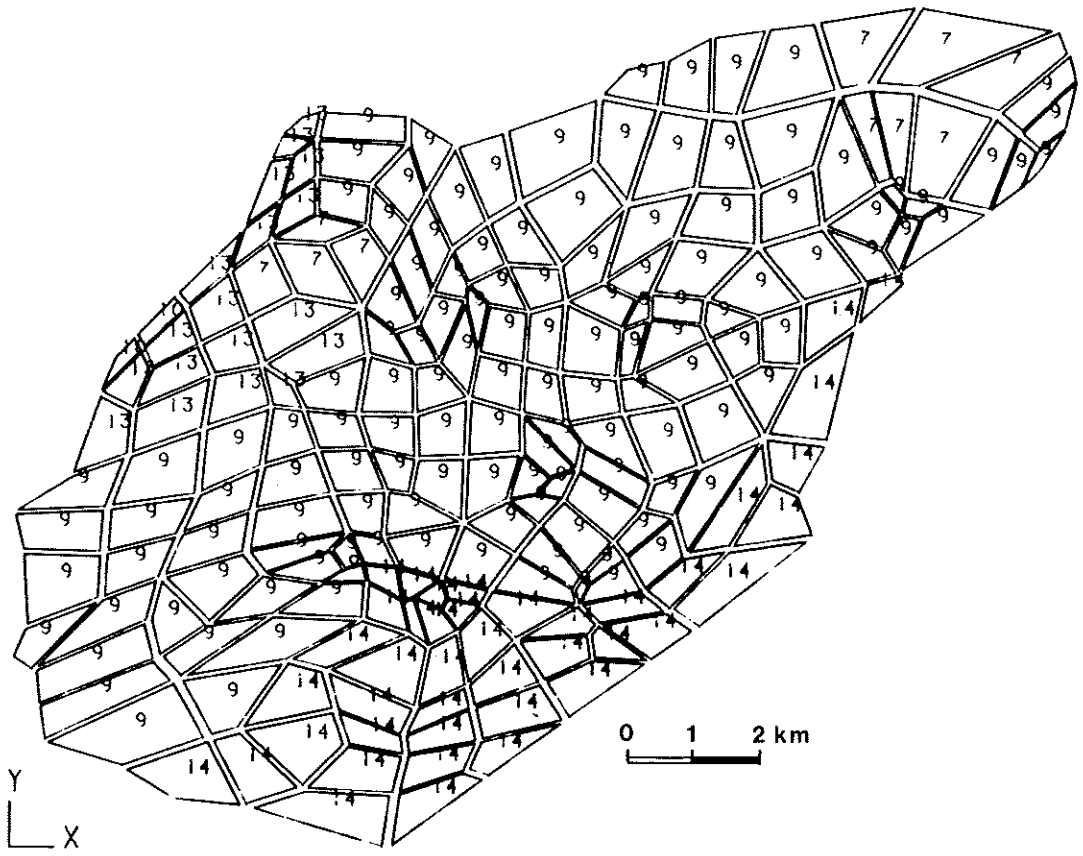

Fig. 14 : 9th layer of elements.

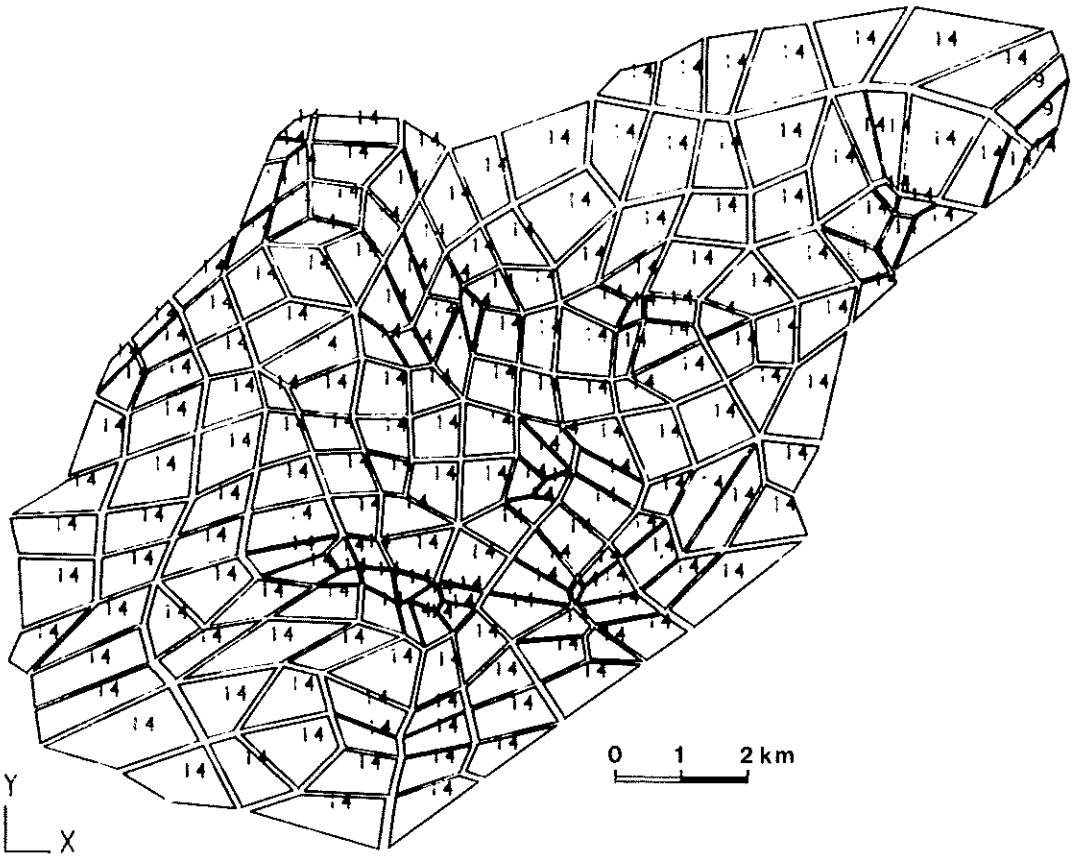

Fig. 15 : 10th layer of elements.

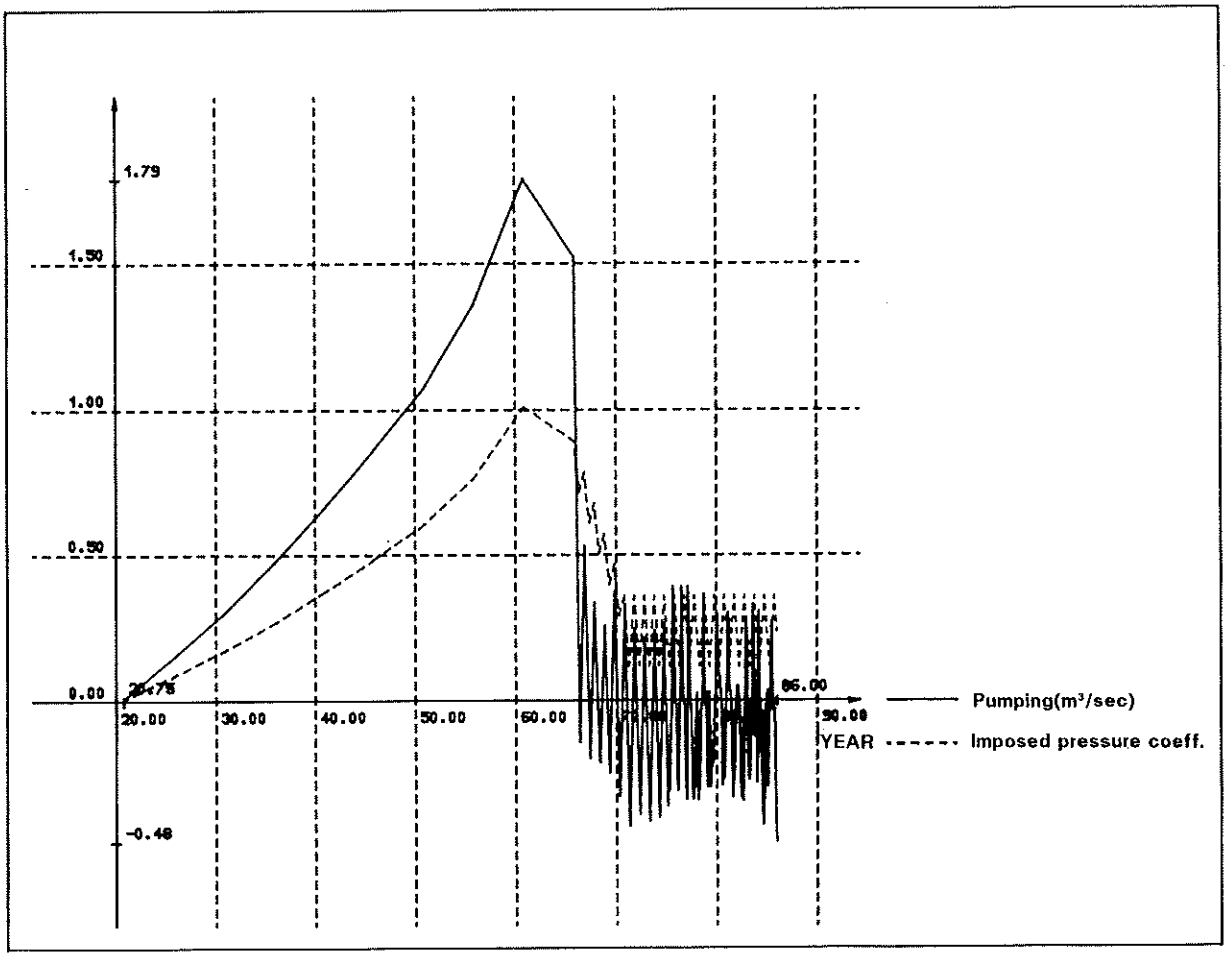

Fig. 16 : Time evolution of the coefficient determining the prescribed pressures on the lateral boundaries compared to the total amount of pumping.

— from 1920.75 to 1965.75 : 9 time steps of 5 years each

— from 1965.75 to 1975.75 : 20 time steps of 6 month each

— from 1975.75 to 1988.75 : 156 time steps of 1 month each

— from 1988.75 to 2000.75 : 144 time steps of 1 month each

This time division is mainly due to the degree of accuracy available in the pumping-recharge data.

From an annual total value about 3.10^5 to 4.10^5 m^3 in 1920, the withdrawal of water increases until a maximum of 56,5 10^6 m^3 in 1960. From this year, annual data are available until 1975. From 1975, the exact date and value of every pumping or recharge are known and recorded in monthly data.

This increasing accuracy with time has motivated the choice of a time-step still shortening with time.

C. Initial conditions and boundary conditions

The piezometric heads of the different aquifers and especially of the second aquifer are not known accurately before 1965. That is why some hypothesis had to be made for the computation of initial data.

A pure hydrostatic initial state with complete saturation of the layers until the surface has been assumed (Fig. 2). This initial state of stress in equilibrium before any pumping, is the only one which can be logically chosen. Any other initial state of the water pressures would suppose that either the Shanghai area was flooded, or that the layers were consolidating by dewatering (not exhibited by the results of the geotechnical tests).

From 1870 to 1920.75, we have let the initial state of stress evolve slowly towards a pressure distribution in equilibrium with the different characteristics of the layers and with the small amount of water initially pumped.

In a first attempt, impervious lateral boundary conditions were considered as an approximation of laterally semi-infinite and horizontal layers in respect to their thickness. Immediately and logically it appeared that the lateral exchanges were not negligible and prescribed head boundaries were introduced (Dirichlet conditions).

These imposed pressure conditions vary with time. The law of variation is directly deduced from the measured pressures in the vicinity of these boundaries and from the pumping rate in the modelled zone. To apply this law in the model, we use in fact a multiplying factor

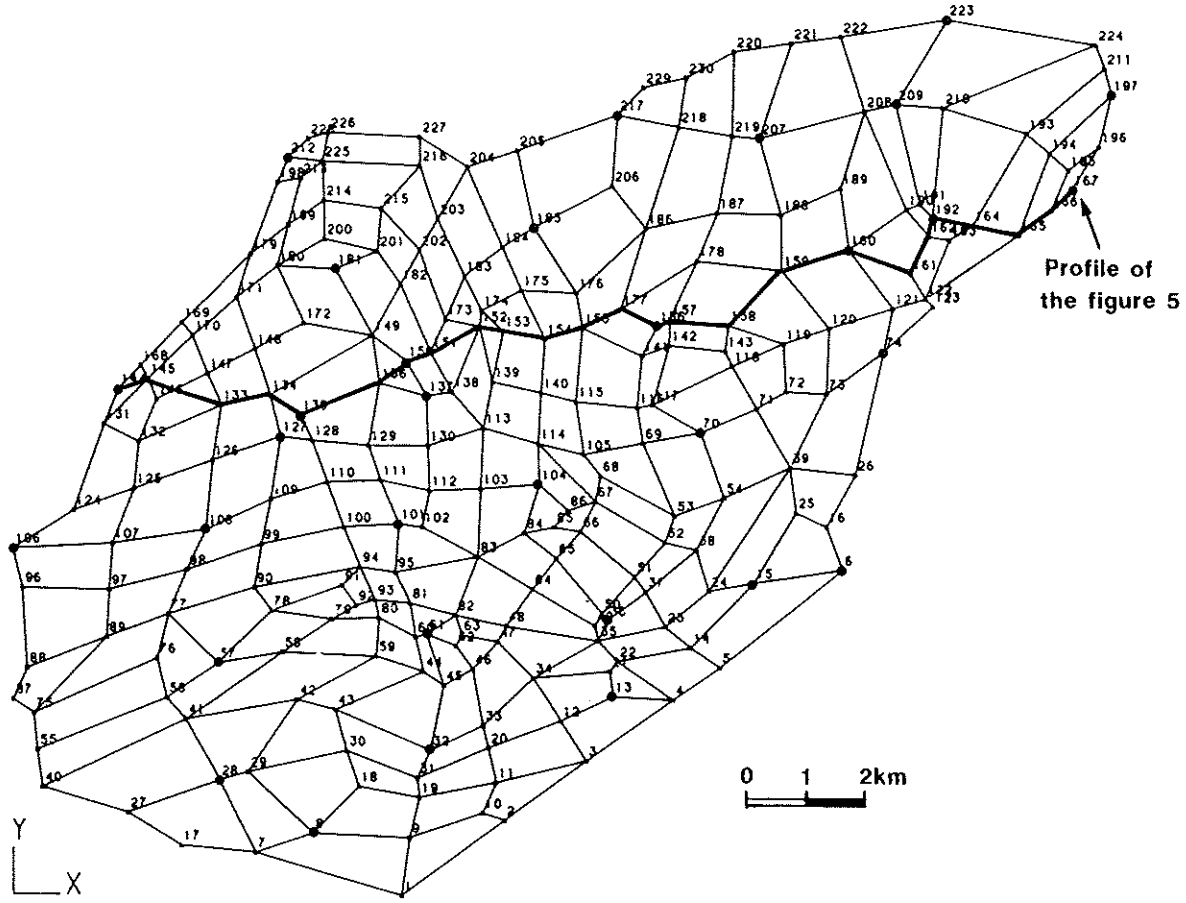

Fig. 17 : Location of the 32 columns.

to the conditions of 1960. The evolution of this coefficient from its maximum value of 1 (1960) is shown on Figure 16.

At the top of the model, we impose a piezometric head equal to the absolute level of the surface, assuming in this way that the water level of the phreatic aquifer is situated very near the soil surface. This condition corresponds to a marshy soil and will introduce a certain amount of natural recharge in the aquifers (situated below) which will depend of the permeability of the clayey layers.

The bottom of the model is considered impervious despite the fact that it is situated everywhere in the 2nd aquifer.

Data of the flow-compaction model

For this study, the subsidence computations are performed using a FEM code, coupling the vertical settlements (geomechanical aspects) and the vertical flows (hydrogeological aspect) in the compressible semi-pervious layers. The simulation is performed while imposing the water pressure, computed by the flow-model, at the aquifer-aquitard boundaries of the modelled columns. These imposed water pressures vary with time.

Moreover, this model composed of many columns takes into account the non-linear variation of the permeability coefficient (K) and specific storage coefficient (S_s). These two parameters are actualized every time step.

The 3D flow model together with the vertical flow-compaction model constitutes a complete 3D analysis of the involved physical phenomena. This analysis takes into account the mainly horizontal flow in aquifers and the mainly vertical and delayed flow and compaction in the compressible semi-pervious layers.

As mentioned above, one dimensional elements with two nodes are chosen; 32 columns have been discretized in the studied zone (Fig. 17).

Each column is composed of 60 elements in order to reach a very good accuracy in the compressible layers. The geomechanical parameters A and C are the essential data which are needed. Additionally, we need the calculated initial void-ratio (e_o) of 1920, the α_N and β_N parameters of the Nishida relation and the effective preconsolidation stress (σ'_{prec}).

The origin of all these data is described in detail in this paper and in the papers above. As an example, the detailed data of the columns 137 and 209 are shown in Tables 2 and 3.

Table 2 : Data of the column 137.

Absolute levels	Elements	Material	A	C	e_o	α	β
+ 3.0 à - 1.3 m	6 de 0.72m	1	8.426D+02	1.053D+02	0.83	7.1	-27.60
- 1.3 à - 3.86m	2 de 1.28m	2	9.030D+02	9.030D+01	0.96	6.7	-27.60
- 3.86 à - 6.42m	2 de 1.28m	3	5.480D+02	6.958D+01	0.91	0.0	-10.82
- 6.42 à - 9.0 m	2 de 2.17m	4	3.001D+02	5.023D+01	1.01	0.0	-10.82
- 9.0 à -13.33m	2 de 2.17m	5	3.930D+01	6.550D+00	1.31	5.5	-27.60
-13.33 à -17.66m	2 de 2.17m	6	2.500D+01	5.000D+00	1.48	5.8	-27.60
-17.66 à -19.89m	1 de 2.17m	7	3.650D+01	6.100D+00	1.17	8.4	-27.60
-19.89 à -25.0 m	1 de 2.17m	8	2.977D+01	5.950D+00	0.82	7.4	-27.60
	6 de 0.5 m	8					
-25.0 à -27.5 m	1 de 2.5 m	9	1.152D+02	1.938D+01	0.85	0.0	-9.90
-27.5 à -30.0 m	1 de 2.5 m	10	1.039D+02	1.039D+01	1.08	0.0	-9.90
-30.0 à -32.5 m	1 de 2.5 m	11	1.567D+02	1.567D+01	1.04	0.0	-9.90
-32.5 à -35.0 m	1 de 2.5 m	12	1.357D+02	1.357D+01	0.95	0.0	-9.90
-35.0 à -37.5 m	1 de 2.5 m	13	1.319D+02	1.319D+01	0.89	0.0	-9.90
-37.5 à -40.0 m	1 de 2.5 m	14	1.430D+02	1.429D+01	1.05	0.0	-9.90
-40.0 à -40.75m	1 de 0.75m	15	6.448D+01	1.283D+01	1.13	7.0	-27.60
-40.75 à -42.25m	2 de 0.75m	16	5.947D+01	1.189D+01	1.15	7.0	-27.60
-42.25 à -44.5 m	3 de 0.75m	17	6.517D+01	1.303D+01	1.07	6.3	-27.60
-44.5 à -46.0 m	2 de 0.75m	18	6.621D+01	1.324D+01	1.10	6.4	-27.60
-46.0 à -49.0 m	4 de 0.75m	19	6.105D+01	1.221D+01	1.10	9.8	-27.60
-49.0 à -50.167	1 de 1.167	20	5.431D+01	1.086D+01	1.13	7.0	-27.60
-50.167à -52.5 m	2 de 1.167	21	6.672D+01	1.112D+01	1.03	6.3	-27.60
-52.5 à -54.83m	2 de 1.167	22	5.216D+01	1.032D+01	1.11	6.4	-27.60
-54.83 à -56.0 m	1 de 1.167	23	6.069D+01	1.007D+01	0.93	5.7	-27.60
-56.0 à -58.33m	2 de 1.167	24	4.890D+01	8.120D+00	0.98	5.7	-27.60
-58.33 à -60.67m	2 de 1.167	25	6.381D+01	1.276D+01	0.94	7.2	-27.60
-60.67 à -63.0 m	2 de 1.167	26	4.576D+01	9.150D+00	0.99	6.3	-27.60
-63.0 à -67.5 m	1 de 4.5 m	27	1.349D+02	2.226D+01	0.94	10.4	-27.60
-67.5 à -72.0 m	1 de 4.5 m	28	5.680D+01	9.430D+00	1.05	7.3	-27.60
-72.0 à -90.0 m	4 de 4.5 m	29	2.925D+02	2.925D+01	0.85	0.0	-7.20

Table 3 : Data of the column 209.

Absolute levels	Elements	material	A	C	e_o	α	β
+ 4.0 à + 0.6 m	6 de 0.57m	1	4.814D+02	6.189D+01	0.88	5.7	-27.6
+ 0.6 à - 2.216m	1 de 2.82m	2	6.911D+02	8.293D+01	0.80	5.7	-27.6
- 2.216à - 5.033m	1 de 2.82m	3	6.329D+01	1.266D+01	1.59	5.7	-27.6
- 5.033à - 7.85 m	1 de 2.82m	4	4.988D+01	9.980D+00	1.43	5.4	-27.6
- 7.85 à -10.66 m	1 de 2.82m	5	3.922D+01	7.840D+00	1.61	5.6	-27.6
- 10.66 à -13.48 m	1 de 2.82m	6	3.712D+01	7.440D+00	1.44	5.7	-27.6
- 13.48 à -16.3 m	1 de 2.82m	7	2.999D+01	6.000D+00	1.48	5.8	-27.6
- 16.3 à -17.6 m	2 de 0.66m	8	2.389D+01	4.050D+00	1.18	7.3	-27.6
- 17.6 à -20.3 m	4 de 0.66m	9	3.748D+01	6.230D+00	1.00	9.2	-27.6
- 20.3 à -25.0 m	6 de 0.78m	10	5.718D+01	7.120D+00	0.89	7.5	-27.6
- 25.0 à -26.47 m	1 de 1.47m	11	1.339D+02	2.209D+01	0.92	6.5	-27.6
- 26.47 à -29.4 m	2 de 1.47m	12	4.813D+01	6.020D+00	0.67	6.5	-27.6
- 29.4 à -32.33 m	2 de 1.47m	13	1.310D+02	2.162D+01	0.88	0.0	-9.9
- 32.33 à -33.8 m	1 de 1.47m	14	1.109D+02	1.109D+01	0.93	0.0	-9.9
- 33.8 à -34.43 m	1 de 0.63m	15	7.227D+01	1.205D+01	0.57	0.0	-9.9
- 34.43 à -41.4 m	5 de 0.63m	16	1.130D+02	1.394D+01	0.82	0.0	-9.9
	6 de 0.63m	16					
- 41.4 à -43.45 m	1 de 2.05m	17	5.845D+01	9.700E+00	1.11	6.5	-27.6
- 43.45 à -45.5 m	1 de 2.05m	18	6.202D+01	1.030D+01	1.24	6.6	-27.6
- 45.5 à -47.55 m	1 de 2.05m	19	6.007D+01	1.021D+01	1.22	6.5	-27.6
- 47.55 à -49.6 m	1 de 2.05m	20	6.650D+01	1.091D+01	1.37	6.6	-27.6
- 49.6 à -51.65 m	1 de 2.05m	21	5.984D+01	1.017D+01	1.21	6.6	-27.6
- 51.65 à -53.7 m	1 de 2.05m	22	5.096D+01	1.009D+01	1.19	7.8	-27.6
- 53.7 à -55.75 m	1 de 2.05m	23	3.863D+01	7.970D+00	1.18	8.2	-27.6
- 55.75 à -57.80 m	1 de 2.05m	24	4.120D+01	8.550D+00	0.97	7.6	-27.6
- 57.80 à -59.85 m	1 de 2.05m	25	4.419D+01	7.370D+00	0.92	8.5	-27.6
- 59.85 à -61.90 m	1 de 2.05m	26	5.354D+01	9.100D+00	0.98	8.7	-27.6
- 61.90 à -63.95 m	1 de 2.05m	27	5.050D+01	8.420D+00	0.98	7.9	-27.6
- 63.95 à -66.00 m	1 de 2.05m	28	5.216D+01	8.660D+00	0.88	8.3	-27.6
- 66.00 à -70.00 m	1 de 4.00m	29	5.108D+01	8.480D+00	1.07	8.1	-27.6
- 70.00 à -74.00 m	1 de 4.00m	30	4.312D+01	7.190D+00	1.06	8.0	-27.6
- 74.00 à -90.00 m	4 de 4.00m	31	2.925D+02	2.925D+01	0.80	0.0	- 7.2

Conclusions

All the data needed in this mathematical simulation have been mentioned and the way to find them has been described. The model was run with these data and the results are fully described in the next paper entitled : "Computed subsidence of the central area of Shanghai" (Dassargues *et al.*).

References

BAETEMAN C., 1989 : The upper Quaternary deposits of the Changjiang coastal plain (Shanghai area). Belgian Geological Survey, unpublished.

BETHKE C.M. and CORBET T.F., 1988 : Linear and Non-linear solutions for one-dimensional compaction flow in sedimentary basins. Water Resources Research. Vol. 24, n° 3, 461-467.

BIVER P., 1988, Simulation numérique de tassements à Shanghai. Travail de fin d'études pour l'obtention du grade d'Ingénieur Civil Géologue à l'Université de Liège.

BREDEHOEFT, J.D. and COOLEY, R.L., 1983, Comment on "A note on the meaning of storage coefficient" by Narasimhan, T.N. and Kanehiro, B.Y., Water Resources Research, Vol. 19, n° 6, 1632-1634.

CORAPCIOGLU M.Y., 1984, Land subsidence. State-of-the-Art review, in Fundamentals of Transport Phenomena in Porous media, edited by Bear J. and Corapcioglu M.Y., NATO ASI Series, Series E : Applied Sciences n° 82 pp. 369-444.

DASSARGUES A., BOLLY P.Y. and MONJOIE A., 1988, Finite difference and finite element modelling of an aquifer in Cretaceous chalk, Proceedings of Numerical Methods in Geomechanics, Innsbruck, Balkema.

DASSARGUES A., CHARLIER R., RADU J.P. et MONJOIE A., 1987, Modélisation de la nappe aquifère de Hesbaye, Rapport L.G.I.H. Université de Liège.

DASSARGUES A., RADU J.R. and CHARLIER R., 1988, Finite element modelling of a large water table aquifer in transient conditions, Advances in water resources, vol. 11, n° 2, pp. 58-66.

DASSARGUES, A., SCHROEDER Ch. and MONJOIE A., 1989, The hydrogeology and engineering geology of the Shanghai area. Laboratoires de Géologie de l'Ingénieur, d'Hydrogéologie et de Prospection géophysique, Rapport SPPS 891, unpublished.

DE MARSILY G., 1981, Hydrogéologie quantitative, Edition Masson.

DE WAAL J.A. and SMITS R.M.M., 1985, Prediction of reservoir compaction and surface subsidence : field application of a new model, Society of Petroleum Engineer (non published).

GHOLAMREZA M. and OLSON R.E., 1971 : Mechanisms controlling the permeability of clays, Clays and Clay Minerals, Vol. 19, 151-158.

MAIN R., CHILINGAR G.V. and SINNOKRAT A., 1963 : Relationship between porosity, permeability and surface area of sediments, Journal of Sedimentary Petrology, Vol. 33, n° 3, 759-765.

NISHIDA Y. and NAKAGAWA S., 1969 : Water permeability and plastic index of soils In : Land Subsidence IAHS-UNESCCO, Publ. n° 89, AIHS (2) : 573-578.

POLAND J.F., 1984 : Mechanics of land subsidence due to fluid withdrawal, in Guidebook to studies of land subsidence due to groundwater withdrawal UNESCO.

RIEKE M.M. and CHILINGARIAN, G.V., 1974 : Compaction of argillaceous Sediments, Elsevier, Amsterdam.

SCHROEDER Ch. and BAETEMAN C., 1990 : Land subsidence in Shanghai. An application of the interaction between coastal-lowland geology and engineering geology, Proc. VIth Int. Cong. of IAEG, Amsterdam, pp. 191-200.

TERZAGHI K. and PECK R., 1948 : Soil mechanics in engineering practice, Wiley and Sons, New-York.

VIDALIE J.F., 1977 : Relations entre les propriétés physicochimiques et les caractéristiques mécaniques des sols compressibles. Rapport de recherche LPC n° 65.